

Relevance to TOGA of Systematic XBT Errors

R.J. BAILEY, H.E. PHILLIPS, G. MEYERS

*CSIRO / Division of Oceanography
GPO Box 1538
Hobart, Tasmania - Australia*

Introduction

Over recent years expendable bathythermographs (XBTs) have become increasingly relied upon in large-scale oceanographic research programs. An assessment of the accuracy of XBTs, and the systems used to drive them, is therefore essential.

The depth accuracy of XBTs has been the subject of many studies ^{1, 2, 3, 4}. These studies have proposed alternative fall-rate equations to the one specified by the manufacturer on the basis of the errors observed in the depth of the XBT. Other investigators ^{5, 6} have concentrated on the temperature calibration of the probe thermistors in an effort to improve the accuracy of XBTs.

The aims of this study are to:

- provide further calibrations of XBTs and XBT systems by comparing them with conductivity-temperature-depth (CTD) sensors.
- evaluate the applicability of the various depth-correction algorithms mentioned above.
- examine the implications of the observed depth and temperature errors to a large-scale research program such as TOGA (Tropical Ocean and Global Atmosphere).

Instrumentation and Methods

Two types of digital XBT systems were calibrated against the RV *Franklin's* Neil Brown CTD Profiler during separate voyages in 1987 (Table 1). Both types of XBT system are used in the CSIRO's Ship-of-Opportunity Program (SOOP). The MK-9 XBT system was used in two configurations for the calibration experiments; with the *Franklin's* PDP-11 data logging system, and with an HP-85 microcomputer as deployed on ships-of-opportunity. Deep Blue XBTs, from the same batch, were used throughout the calibrations.

The CTD station positions are shown in Fig. 1. Typically, XBTs were dropped 10-20 minutes prior to the descent of the CTD profiler at each station.

The temperature profiles recorded by the CTD Profiler for both voyages are shown in Fig. 2.



Table 1

Calibration Experiment #	Voyage	XBT System Description	XBT Type	Number of XBTs	Number of Corresponding CTDs
1	FR0487	SEAS II/Bathy Systems SA-810 (HP-85)	Deep Blue	17	17
2	FR1087	Sippican MK-9 (HP-85)	Deep Blue	14	3
3	FR1087	Sippican MK-9 (PDP-11)	Deep Blue	12	3

Table 2

DYNAMIC HEIGHT ERROR

Voyage	XBT System	Error in Dynamic Height Relative to 200 m (dyn m)		Error in Dynamic Height Relative to 400 m (dyn m)		Error in Dynamic Height Relative to 700 m (dyn m)	
		Mean	Standard Dev.	Mean	Standard Dev.	Mean	Standard Dev.
FR0487	SEAS II/Bathy Systems SA-810 (HP-85)	0.001 (0.007)	0.007 (0.008)	-0.009 (0.010)	0.013 (0.013)	-0.012 (0.020)	0.013 (0.014)
FR1087	Sippican MK-9 (HP-85)	-0.011 (0.004)	0.007 (0.006)	-0.012 (0.011)	0.009 (0.009)	-0.016 (0.012)	0.011 (0.011)
FR1087	Sippican MK-9 (PDP-11)	-0.011 (0.003)	0.008 (0.009)	-0.013 (0.008)	0.008 (0.008)	-0.019 (0.009)	0.012 (0.011)

() after XBT depth correction according to Hanawa and Yoritaka⁴.

Table 3

SEAS II MIXED LAYER ANOMALY ANALYSIS 1987
(Estimate)

$$\text{Index} = T_{\max} - T_{5 \text{ metres}}$$

Total number of drops = 1739

Total number of anomalous drops = 1223

Mean Index for anomalous drops = 0.22

Index Bin	Index >	Range ≤	Frequency	Percentage of Total Drops
0.1	0.05	0.15	625	35.94
0.2	0.15	0.25	315	18.12
0.3	0.25	0.35	133	7.65
0.4	0.35	0.45	44	2.53
≥0.5	0.45	—	106	6.10
			TOTAL = 1223	TOTAL = 70.34

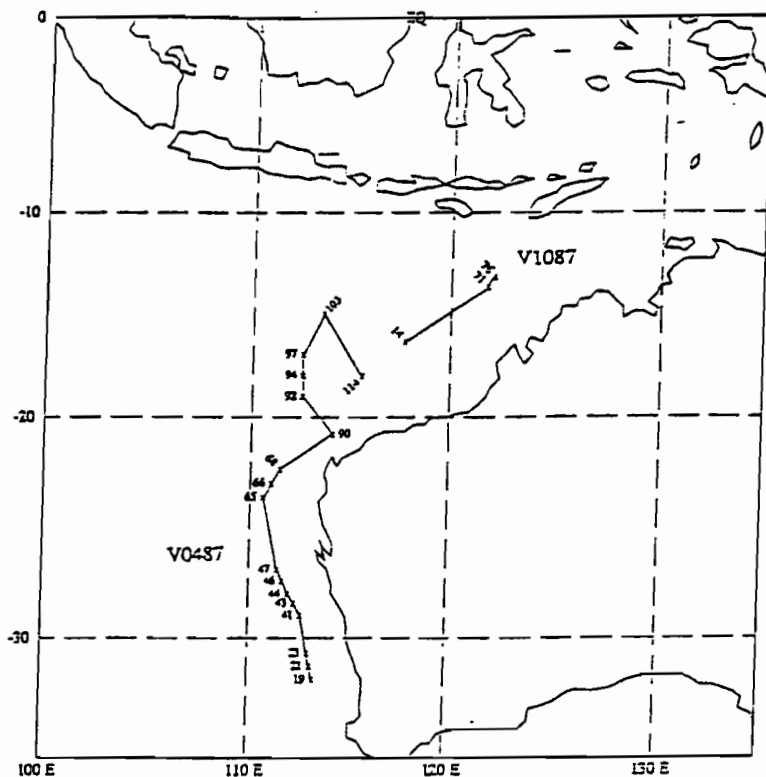


FIG.1. RV Franklin V0487 and V1087 station positions.

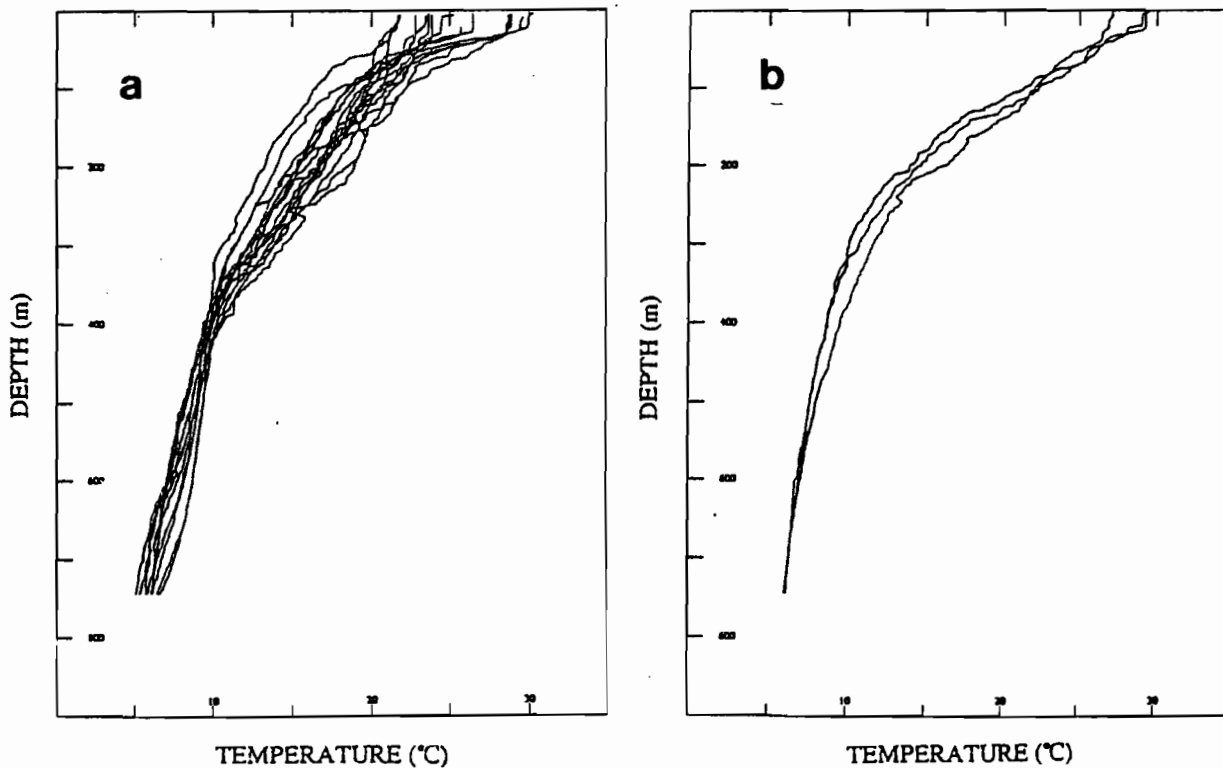


FIG.2. CTD temperature profiles: (a) FR0487, (b) FR1087

Depth and Temperature Errors

(a) Depth Errors

Figs. 3(a) and 4(a) give examples of the average temperature error ($T_{\text{XBT}} - T_{\text{CTD}}$) as a function of depth for two of the XBT System/CTD calibration experiments. The characteristic shape of both profiles of temperature error is similar to that found in the experiments of Hanawa and Yoritaka⁴. They found the negative errors in temperature to be mainly due to the errors in depth that result from the XBT falling faster than specified by the manufacturer's fall-rate equation. The largest errors in temperature correspond to the depths of large temperature gradient in the temperature profiles (cf Fig. 2). This is where the depth error due to an incorrect fall-rate has its largest effect.

Figs 3(b) and 4(b) give examples of the average temperature error ($T_{\text{XBT}} - T_{\text{CTD}}$) as a function of depth for the same two calibration experiments, however, the depths of the XBTs have been corrected according to the depth-correction algorithm developed by Hanawa and Yoritaka⁴. This algorithm proved to be the most successful at reducing the mean and rms temperature errors for each of the three calibration experiments. The rms temperature error was consistently reduced from above to below the accuracy of the XBT ($\pm 0.15^\circ\text{C}$). The depth-correction algorithm according to Heinmiller et al.¹, on the other hand, actually increased the rms temperature error for each case.

Unfortunately, some errors in temperature still remain at depths corresponding to large temperature gradients, even after the data has been corrected according to Hanawa and Yoritaka⁴. The fall-rate correction of Hanawa and Yoritaka⁴ is therefore not totally applicable in the waters of this study, although it does improve the data.

(b) Temperature Errors

Start-up Transients: Large start-up transients in the upper 4 m were observed for the SEAS II XBT System (Fig. 5), and to a lesser extent for the MK-9 XBT System. The mean difference between the first temperature digitisation (0.6 m) and the temperature at 3.9 m (commonly used as the sea surface temperature due to such transients) was $-9.50 \pm 10.08^\circ\text{C}$ for the SEAS II XBT System, compared to $0.41 \pm 0.30^\circ\text{C}$ for the MK-9 XBT System.

SEAS II Mixed Layer Anomaly (Bowling): The need for the comparison of XBT data with a precision CTD sensor was first invoked by the observation of anomalies in the mixed layer temperature profiles recorded by SEAS II XBT Systems deployed in the CSIRO SOOP in the western tropical Pacific. A gradual increase, or "bowing", in temperature was observed as opposed to an isothermal profile. An example is given in Fig. 6. Such anomalies were not present in the data recorded by the MK-9 XBT Systems.

The upper 200 m of the temperature profiles recorded by the SEAS II XBT System and the CTD Profiler during FR0487 are shown in Figs 7(a) and 7(b) respectively. The gradient in temperature in the mixed layer for a single XBT and its corresponding CTD are highlighted to emphasize the "bowing" problem. The corresponding average error in temperature ($T_{\text{XBT}} - T_{\text{CTD}}$) in the mixed layer as a function of depth is shown in Fig. 7(c). The mean SEAS II XBT temperature in the mixed layer starts less than and finishes greater than the mixed layer temperature given by the CTD. On examination of each individual XBT/CTD

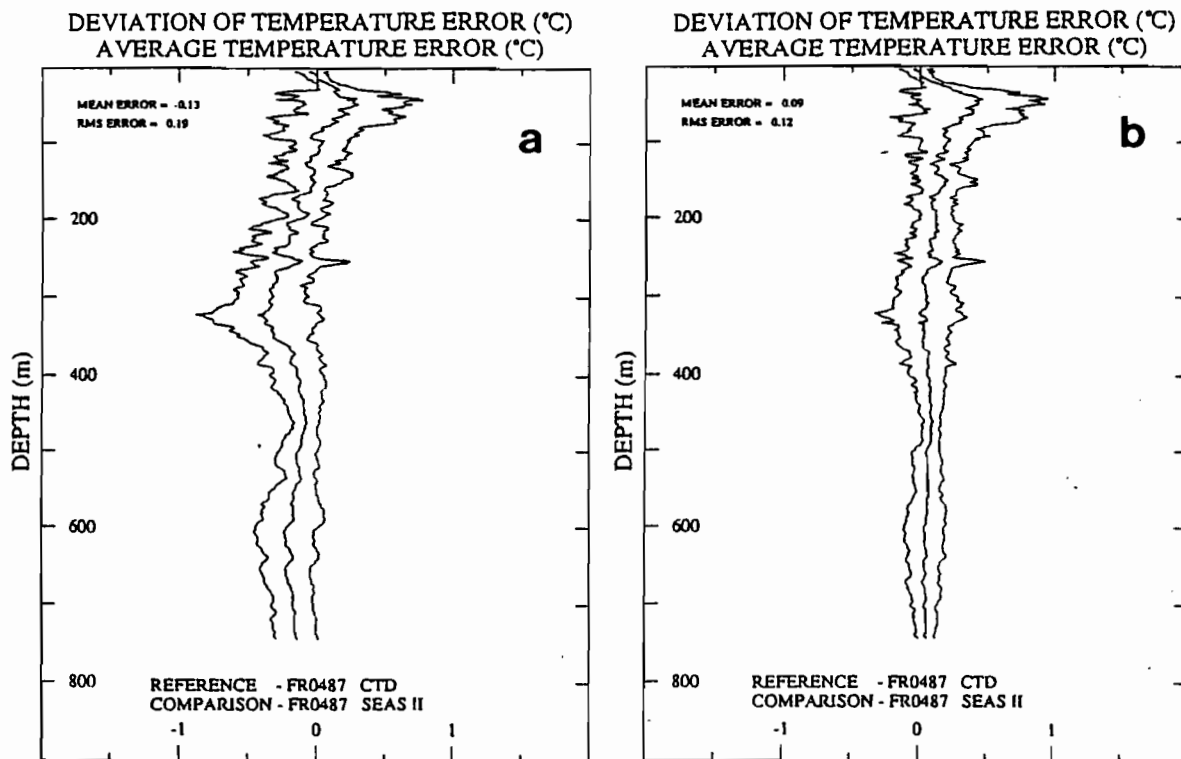


FIG.3. Average temperature error profiles (TXBT-TCTD) for the XBT/CTD comparisons on FR0487 using the SEAS II XBT system; (a) depth uncorrected, (b) depth corrected according to Hanawa and Yoritaka4.

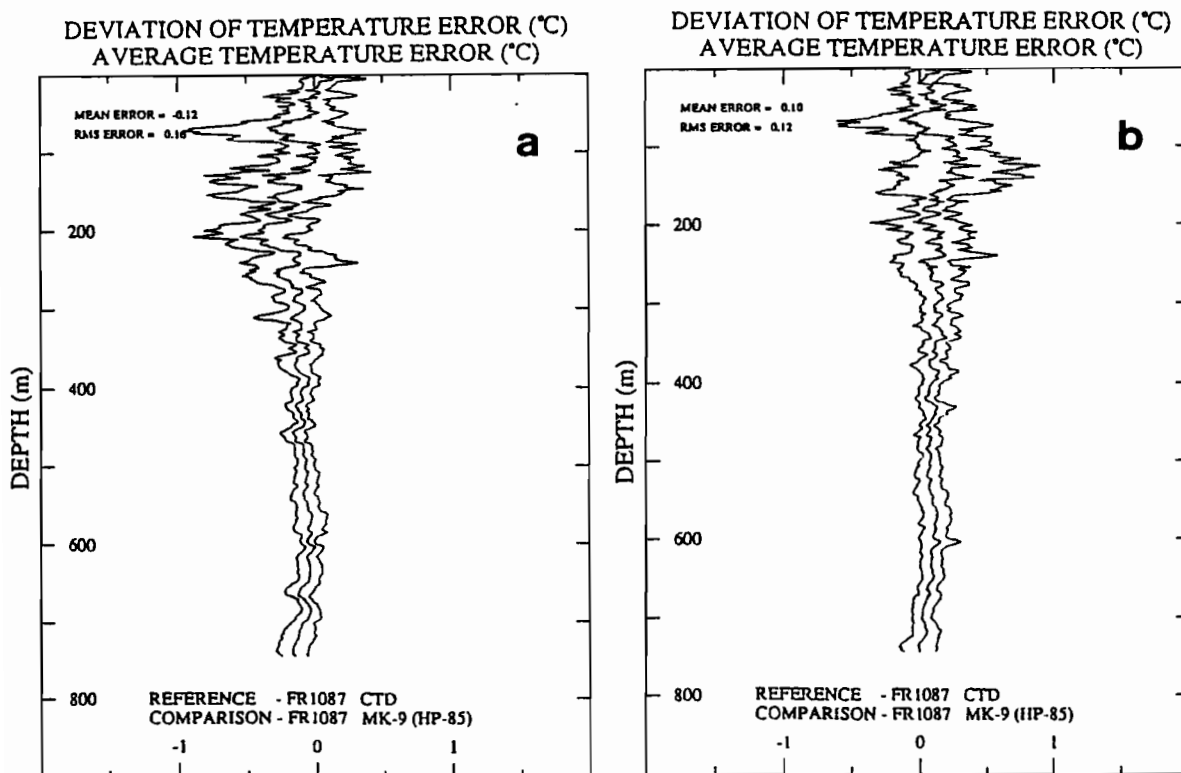


FIG.4. Average temperature error profiles (TXBT-TCTD) for the XBT/CTD comparisons on FR1087 using the MK-9 XBT system; (a) depth uncorrected, (b) depth corrected according to Hanawa and Yoritaka4.

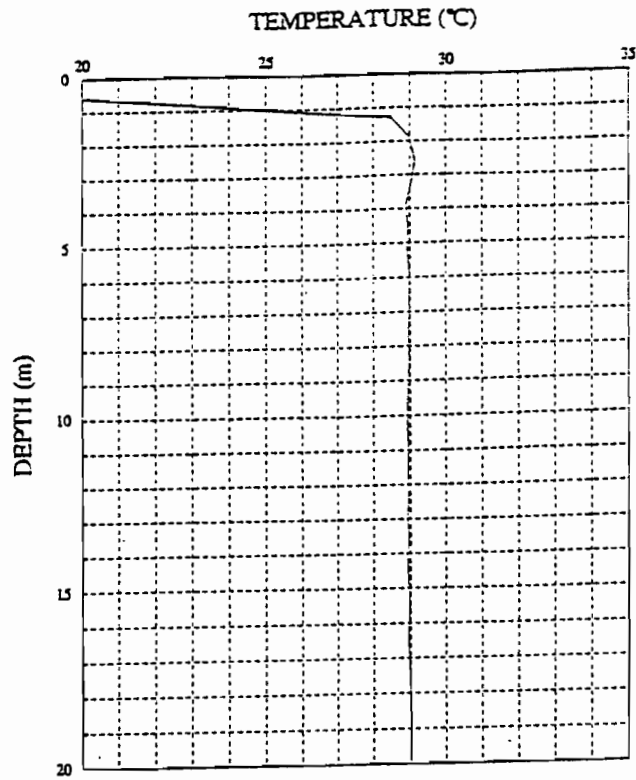


FIG.5. Example of a start-up transient from a SEAS II XBT system.

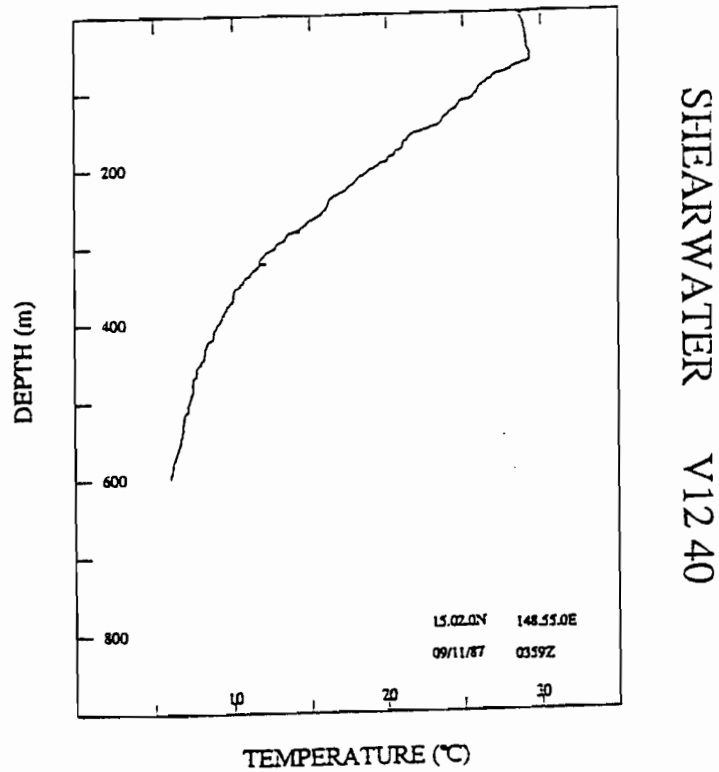


FIG.6. Example of a mixed layer anomaly recorded by a SEAS II XBT system.

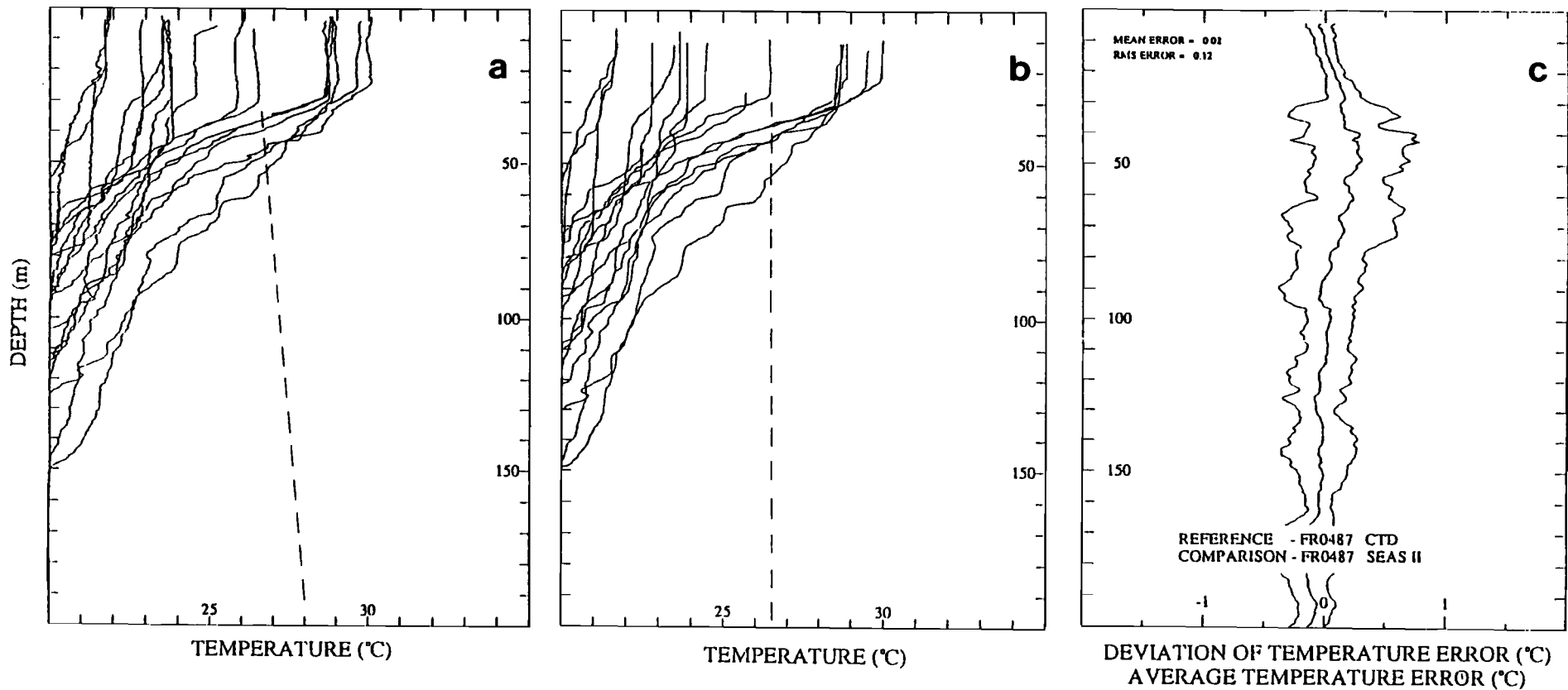


Fig. 7. (a) SEAS II temperature profiles (upper 200 m) for FR0487; (b) CTD temperature profiles (upper 200 m) for FR0487; (c) corresponding average temperature error profile (upper 200 m)

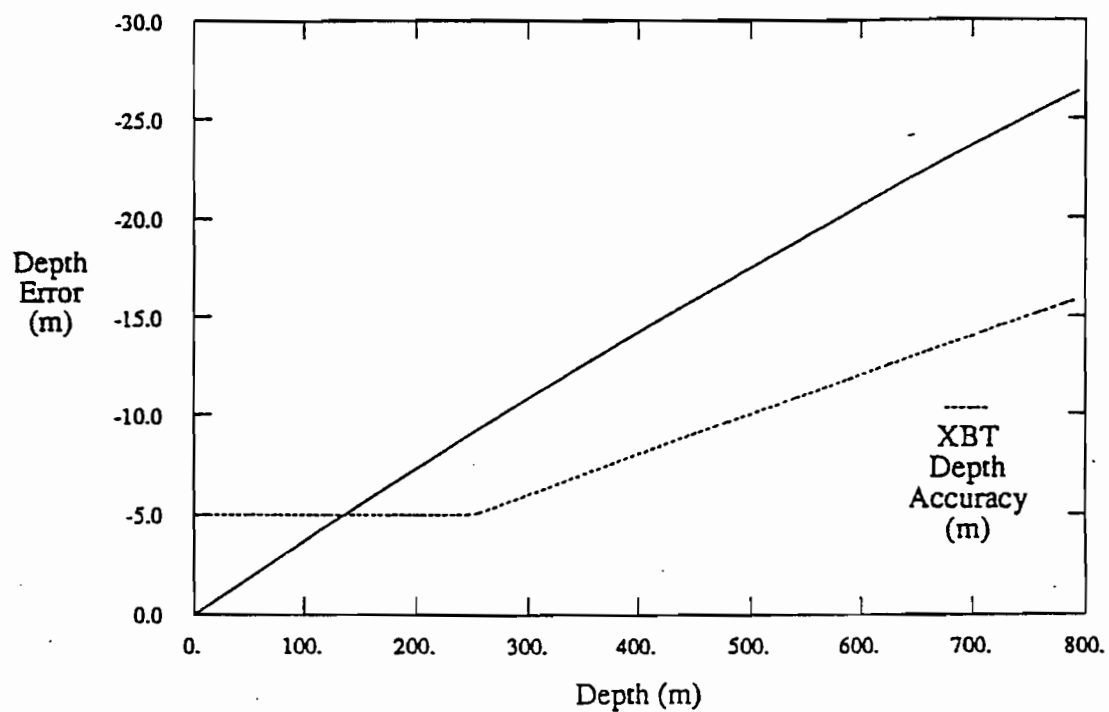


FIG.8. Depth error of the XBT as a function of depth.

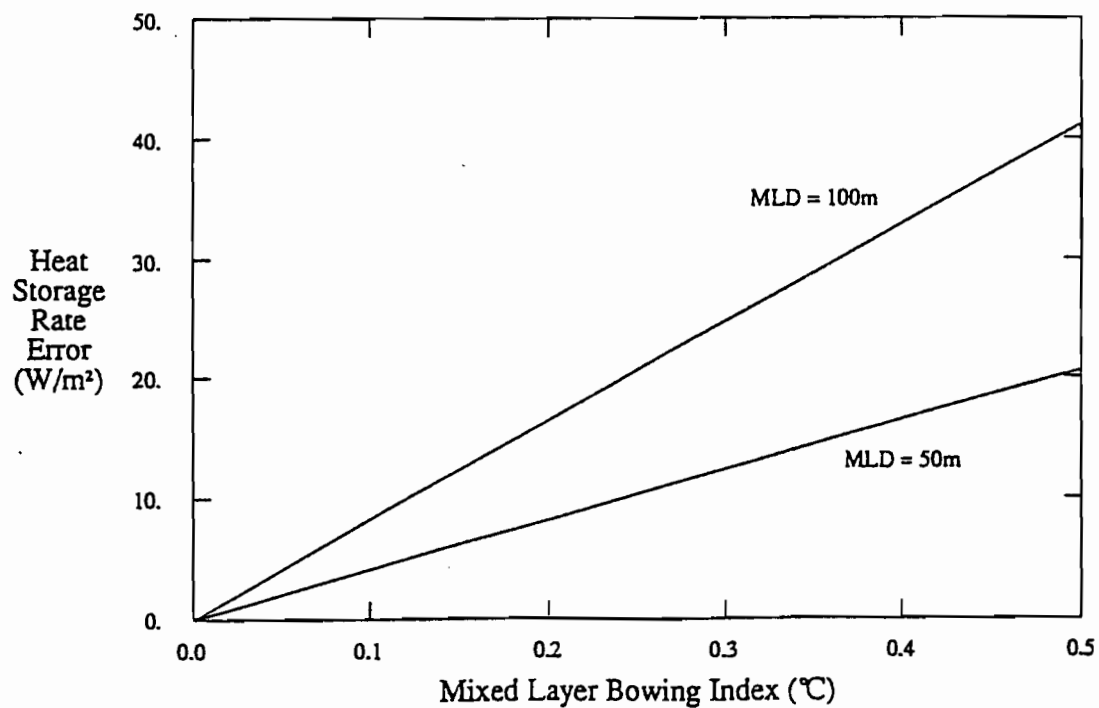


FIG.9. Error in monthly heat storage rate due to the "bowing" problem of the SEAS II XBT system.

comparison, however, the start and finish temperatures of the SEAS II XBT System were found to be randomly distributed in relation to the CTD mixed layer temperature. In some cases the SEAS II temperature starts above the CTD mixed layer temperature and finishes further above it. In other cases, it may start below it and finish equal to it.

The above results indicate a possible drift problem with the electronics of the SEAS II XBT System. The temperature errors may also extend deeper than the mixed layer. We can only distinguish the problem in the mixed layer where the real temperature gradient is zero.

Implications for TOGA

(a) *Isotherm Depth Errors*

If we assume the corrected depth (z') from Hanawa and Yoritaka⁴ to be the true depth of the XBT, then Fig. 8 shows the depth error ($z-z'$) as a function of depth, where z is the depth of the XBT given by the manufacturer. The depth accuracy of the XBT at any given depth is also shown. A 20°C isotherm depth of 200 m, for example, will be measured by an XBT as occurring at a depth of approximately 192.5 m — an error of 7.5 m. The depth error exceeds 25 m at a depth of 800 m, and exceeds the depth accuracy of the XBT (5 m or 2% of the depth, whichever is greater) at a depth of approximately 135 m.

(b) *Dynamic Height Errors*

Table 2 shows the mean error in dynamic height ($D_{\text{XBT}}-D_{\text{CTD}}$) relative to 200 m, 400 m and 700 m for the three calibration experiments. The errors are small both before and after the correction for depth of the XBT. Values range from -0.019 dyn m to 0.001 dyn m. Fortunately, the largest temperature gradients in the tropics are shallow enough for errors in temperature, which affect the dynamic height, to be small. The error in depth, which affects the temperature error, is relatively small at these shallower depths.

The depth correction from Hanawa and Yoritaka⁴ successfully reduces the error in dynamic height for the MK-9 XBT System, but increases it for the SEAS II XBT System. The additional positive errors in temperature caused by the “bowing” problem of the SEAS II XBT System are possibly cancelling some of the negative errors in temperature that result from errors in depth. The dynamic height error, which depends on temperature, is therefore reduced for the SEAS II XBT System.

(c) *Mixed Layer Temperature Errors*

A mixed layer bowing index, defined as the maximum temperature of a profile minus the temperature at 5 m, was used to estimate the typical magnitude and frequency of the mixed layer anomaly recorded by the SEAS II XBT Systems deployed in the CSIRO SOOP. The results for the XBT data recorded in 1987 are given in Table 3. Potentially, 34.4% of the data had errors greater than the temperature accuracy of the XBT ($\pm 0.15^\circ\text{C}$). Some profiles recorded indexes of 0.7°C (Fig. 6) and above.

Fig. 9 shows the error in monthly heat storage rates as a function of the potential error in mixed layer temperature due to "bowing". The errors are shown for two characteristic mixed layer depths (MLD). Given the mean index for 1987 from Table 3 of 0.22°C , the corresponding error in the monthly heat storage rate is approximately 18 W/m^2 for a mixed layer depth of 100 m. This is an unacceptable source of error in heat budget studies.

(d) *Sea Surface Temperature Errors*

The shallowest depth that should be used to estimate sea surface temperature (SST) from an XBT is 3.9 m due to start-up transients. Large errors in SST will be observed otherwise.

Conclusions

- The depth-correction algorithm according to Hanawa and Yoritaka⁴ proved the most effective in reducing the mean and rms temperature errors for this data set. However, as neither this correction nor the other corrections that were applied completely reduced the temperature errors observed between the XBTs and CTD Profiler, further studies on the factors that vary the fall-rate of XBTs between different locations will need to be undertaken before a generally applicable depth-correction algorithm will be found. This will have to be done for each type of XBT probe.
- Temperature errors observed in the mixed layer, due to the "bowing" problem associated with the SEAS II XBT System, are a significant source of error for TOGA. A thorough engineering analysis of the electronics of this system is recommended before future use of the system. On the results of this study, CSIRO has replaced the SEAS II units in its SOOP with MK-9 XBT Systems.

References

1. Heinmiller, R., C. Ebbesmeyer, B. Taft, D. Olson and O. Nikitin (1983): Systematic errors in expendable bathythermograph (XBT) profiles. *Deep-sea Research* **30**, 1185-1196.
2. Seaver, G., and S. Kuleshov (1982): Experimental and analytical error of the expendable bathythermograph. *Journal of Physical Oceanography* **12**, 592-600.
3. Green, A. (1984): Bulk dynamics of the expendable bathythermograph (XBT). *Deep-sea Research* **31**, 415-426.
4. Hanawa, K. and H. Yoritaka (1987): Detection of systematic errors in XBT data and their correction. *Journal of the Oceanographical Society of Japan* **43**, 68-76.
5. Georgi, D., J. Dean and J. Chase (1980): Temperature calibration of expendable bathythermographs. *Ocean Engineering* **7**, 491-499.
6. Roemmich, D. and B. Cornuelle (1987): Digitisation and calibration of the expendable bathythermograph. *Deep-sea Research* **34**, 299-307.

**WESTERN PACIFIC INTERNATIONAL MEETING
AND WORKSHOP ON TOGA COARE**

Nouméa, New Caledonia

May 24-30, 1989

PROCEEDINGS

edited by

Joël Picaut *

Roger Lukas **

Thierry Delcroix *

* ORSTOM, Nouméa, New Caledonia

** JIMAR, University of Hawaii, U.S.A.

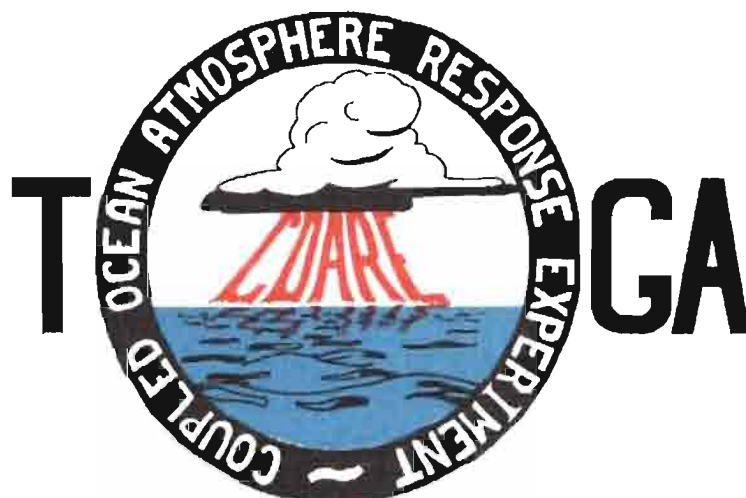


TABLE OF CONTENTS

ABSTRACT	i
RESUME	iii
ACKNOWLEDGMENTS	vi
INTRODUCTION	
1. Motivation	1
2. Structure	2
LIST OF PARTICIPANTS	5
AGENDA	7
WORKSHOP REPORT	
1. Introduction	19
2. Working group discussions, recommendations, and plans	20
a. Air-Sea Fluxes and Boundary Layer Processes	20
b. Regional Scale Atmospheric Circulation and Waves	24
c. Regional Scale Oceanic Circulation and Waves	30
3. Related programs	35
a. NASA Ocean Processes and Satellite Missions	35
b. Tropical Rainfall Measuring Mission	37
c. Typhoon Motion Program	39
d. World Ocean Circulation Experiment	39
4. Presentations on related technology	40
5. National reports	40
6. Meeting of the International Ad Hoc Committee on TOGA COARE	40
APPENDIX: WORKSHOP RELATED PAPERS	
Robert A. Weller and David S. Hosom: Improved Meteorological Measurements from Buoys and Ships for the World Ocean Circulation Experiment	45
Peter H. Hildebrand: Flux Measurement using Aircraft and Radars	57
Walter F. Dabberdt, Hale Cole, K. Gage, W. Ecklund and W.L. Smith: Determination of Boundary-Layer Fluxes with an Integrated Sounding System	81

MEETING COLLECTED PAPERS

WATER MASSES, SEA SURFACE TOPOGRAPHY, AND CIRCULATION

Klaus Wyrtki: Some Thoughts about the West Pacific Warm Pool	99
Jean René Donguy, Gary Meyers, and Eric Lindstrom: Comparison of the Results of two West Pacific Oceanographic Expeditions FOC (1971) and WEPOCS (1985-86)	111
Dunxin Hu, and Maochang Cui: The Western Boundary Current in the Far Western Pacific Ocean	123
Peter Hacker, Eric Firing, Roger Lukas, Philipp L. Richardson, and Curtis A. Collins: Observations of the Low-latitude Western Boundary Circulation in the Pacific during WEPOCS III	135
Stephen P. Murray, John Kindle, Dharma Arief, and Harley Hurlburt: Comparison of Observations and Numerical Model Results in the Indonesian Throughflow Region	145
Christian Henin: Thermohaline Structure Variability along 165°E in the Western Tropical Pacific Ocean (January 1984 - January 1989)	155
David J. Webb, and Brian A. King: Preliminary Results from Charles Darwin Cruise 34A in the Western Equatorial Pacific	165
Warren B. White, Nicholas Graham, and Chang-Kou Tai: Reflection of Annual Rossby Waves at The Maritime Western Boundary of the Tropical Pacific	173
William S. Kessler: Observations of Long Rossby Waves in the Northern Tropical Pacific	185
Eric Firing, and Jiang Songnian: Variable Currents in the Western Pacific Measured During the US/PRC Bilateral Air-Sea Interaction Program and WEPOCS	205
John S. Godfrey, and A. Weaver: Why are there Such Strong Steric Height Gradients off Western Australia ?	215
John M. Toole, R.C. Millard, Z. Wang, and S. Pu: Observations of the Pacific North Equatorial Current Bifurcation at the Philippine Coast	223

EL NINO/SOUTHERN OSCILLATION 1986-87

Gary Meyers, Rick Bailey, Eric Lindstrom, and Helen Phillips: Air/Sea Interaction in the Western Tropical Pacific Ocean during 1982/83 and 1986/87	229
Laury Miller, and Robert Cheney: GEOSAT Observations of Sea Level in the Tropical Pacific and Indian Oceans during the 1986-87 El Nino Event	247
Thierry Delcroix, Gérard Eldin, and Joël Picaut: GEOSAT Sea Level Anomalies in the Western Equatorial Pacific during the 1986-87 El Nino, Elucidated as Equatorial Kelvin and Rossby Waves	259
Gérard Eldin, and Thierry Delcroix: Vertical Thermal Structure Variability along 165°E during the 1986-87 ENSO Event	269
Michael J. McPhaden: On the Relationship between Winds and Upper Ocean Temperature Variability in the Western Equatorial Pacific	283

John S. Godfrey, K. Ridgway, Gary Meyers, and Rick Bailey: Sea Level and Thermal Response to the 1986-87 ENSO Event in the Far Western Pacific	291
Joël Picaut, Bruno Camusat, Thierry Delcroix, Michael J. McPhaden, and Antonio J. Busalacchi: Surface Equatorial Flow Anomalies in the Pacific Ocean during the 1986-87 ENSO using GEOSAT Altimeter Data	301

THEORETICAL AND MODELING STUDIES OF ENSO AND RELATED PROCESSES

Julian P. McCreary, Jr.: An Overview of Coupled Ocean-Atmosphere Models of El Nino and the Southern Oscillation	313
Kensuke Takeuchi: On Warm Rossby Waves and their Relations to ENSO Events	329
Yves du Penhoat, and Mark A. Cane: Effect of Low Latitude Western Boundary Gaps on the Reflection of Equatorial Motions	335
Harley Hurlburt, John Kindle, E. Joseph Metzger, and Alan Wallcraft: Results from a Global Ocean Model in the Western Tropical Pacific	343
John C. Kindle, Harley E. Hurlburt, and E. Joseph Metzger: On the Seasonal and Interannual Variability of the Pacific to Indian Ocean Throughflow	355
Antonio J. Busalacchi, Michael J. McPhaden, Joël Picaut, and Scott Springer: Uncertainties in Tropical Pacific Ocean Simulations: The Seasonal and Interannual Sea Level Response to Three Analyses of the Surface Wind Field	367
Stephen E. Zebiak: Intraseasonal Variability - A Critical Component of ENSO ?	379
Akimasa Sumi: Behavior of Convective Activity over the "Jovian-type" Aqua-Planet Experiments	389
Ka-Ming Lau: Dynamics of Multi-Scale Interactions Relevant to ENSO	397
Pecheng C. Chu and Roland W. Garwood, Jr.: Hydrological Effects on the Air-Ocean Coupled System	407
Sam F. Iacobellis, and Richard C.J. Somerville: A one Dimensional Coupled Air-Sea Model for Diagnostic Studies during TOGA-COARE	419
Allan J. Clarke: On the Reflection and Transmission of Low Frequency Energy at the Irregular Western Pacific Ocean Boundary - a Preliminary Report	423
Roland W. Garwood, Jr., Pecheng C. Chu, Peter Muller, and Niklas Schneider: Equatorial Entrainment Zone : the Diurnal Cycle	435
Peter R. Gent: A New Ocean GCM for Tropical Ocean and ENSO Studies	445
Wasito Hadi, and Nuraini: The Steady State Response of Indonesian Sea to a Steady Wind Field	451
Pedro Ripa: Instability Conditions and Energetics in the Equatorial Pacific	457
Lewis M. Rothstein: Mixed Layer Modelling in the Western Equatorial Pacific Ocean	465
Neville R. Smith: An Oceanic Subsurface Thermal Analysis Scheme with Objective Quality Control	475
Duane E. Stevens, Qi Hu, Graeme Stephens, and David Randall: The hydrological Cycle of the Intraseasonal Oscillation	485
Peter J. Webster, Hai-Ru Chang, and Chidong Zhang: Transmission Characteristics of the Dynamic Response to Episodic Forcing in the Warm Pool Regions of the Tropical Oceans	493

MOMENTUM, HEAT, AND MOISTURE FLUXES BETWEEN ATMOSPHERE AND OCEAN

W. Timothy Liu: An Overview of Bulk Parametrization and Remote Sensing of Latent Heat Flux in the Tropical Ocean	513
E. Frank Bradley, Peter A. Coppin, and John S. Godfrey: Measurements of Heat and Moisture Fluxes from the Western Tropical Pacific Ocean	523
Richard W. Reynolds, and Ants Leetmaa: Evaluation of NMC's Operational Surface Fluxes in the Tropical Pacific	535
Stanley P. Hayes, Michael J. McPhaden, John M. Wallace, and Joël Picaut: The Influence of Sea-Surface Temperature on Surface Wind in the Equatorial Pacific Ocean	543
T.D. Keenan, and Richard E. Carbone: A Preliminary Morphology of Precipitation Systems In Tropical Northern Australia	549
Phillip A. Arkin: Estimation of Large-Scale Oceanic Rainfall for TOGA	561
Catherine Gautier, and Robert Frouin: Surface Radiation Processes in the Tropical Pacific	571
Thierry Delcroix, and Christian Henin: Mechanisms of Subsurface Thermal Structure and Sea Surface Thermo-Haline Variabilities in the South Western Tropical Pacific during 1979-85 - A Preliminary Report	581
Greg. J. Holland, T.D. Keenan, and M.J. Manton: Observations from the Maritime Continent : Darwin, Australia	591
Roger Lukas: Observations of Air-Sea Interactions in the Western Pacific Warm Pool during WEPOCS	599
M. Nunez, and K. Michael: Satellite Derivation of Ocean-Atmosphere Heat Fluxes in a Tropical Environment	611

EMPIRICAL STUDIES OF ENSO AND SHORT-TERM CLIMATE VARIABILITY

Klaus M. Weickmann: Convection and Circulation Anomalies over the Oceanic Warm Pool during 1981-1982	623
Claire Perigaud: Instability Waves in the Tropical Pacific Observed with GEOSAT	637
Ryuichi Kawamura: Intraseasonal and Interannual Modes of Atmosphere-Ocean System Over the Tropical Western Pacific	649
David Gutzler, and Tamara M. Wood: Observed Structure of Convective Anomalies	659
Siri Jodha Khalsa: Remote Sensing of Atmospheric Thermodynamics in the Tropics	665
Bingrong Xu: Some Features of the Western Tropical Pacific: Surface Wind Field and its Influence on the Upper Ocean Thermal Structure	677
Bret A. Mullan: Influence of Southern Oscillation on New Zealand Weather	687
Kenneth S. Gage, Ben Basley, Warner Ecklund, D.A. Carter, and John R. McAfee: Wind Profiler Related Research in the Tropical Pacific	699
John Joseph Bates: Signature of a West Wind Convective Event in SSM/I Data	711
David S. Gutzler: Seasonal and Interannual Variability of the Madden-Julian Oscillation	723
Marie-Hélène Radenac: Fine Structure Variability in the Equatorial Western Pacific Ocean	735
George C. Reid, Kenneth S. Gage, and John R. McAfee: The Climatology of the Western Tropical Pacific: Analysis of the Radiosonde Data Base	741

Chung-Hsiung Sui, and Ka-Ming Lau: Multi-Scale Processes in the Equatorial Western Pacific	747
Stephen E. Zebiak: Diagnostic Studies of Pacific Surface Winds	757

MISCELLANEOUS

Rick J. Bailey, Helene E. Phillips, and Gary Meyers: Relevance to TOGA of Systematic XBT Errors	775
Jean Blanchot, Robert Le Borgne, Aubert Le Bouteiller, and Martine Rodier: ENSO Events and Consequences on Nutrient, Planktonic Biomass, and Production in the Western Tropical Pacific Ocean	785
Yves Dandonneau: Abnormal Bloom of Phytoplankton around 10°N in the Western Pacific during the 1982-83 ENSO	791
Cécile Dupouy: Sea Surface Chlorophyll Concentration in the South Western Tropical Pacific, as seen from NIMBUS Coastal Zone Color Scanner from 1979 to 1984 (New Caledonia and Vanuatu)	803
Michael Szabados, and Darren Wright: Field Evaluation of Real-Time XBT Systems	811
Pierre Rual: For a Better XBT Bathy-Message: Onboard Quality Control, plus a New Data Reduction Method	823